Fuel 379 (2025) 133042

Contents lists available at ScienceDirect

Fuel

journal homepage: www.elsevier.com/locate/fuel

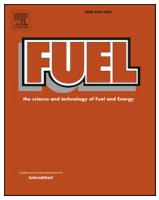

Full Length Article

Numerical analysis of the scavenging process in a large Two-Stroke engine using varied turbulence models

Flora Razavirad [a,b,*], Bjørn Christian Dueholm [a], Nikolaj Kristensen [b], Jesper de Claville Christiansen [a]

[a] Department of Materials and Production, Aalborg University, Pontoppidanstræde 103, 9220 Aalborg East, Denmark
[b] Hans Jensen Lubricators A/S, Smedevænget 3, 9560 Hadsund, Denmark

ARTICLE INFO

Keywords:
Two-stroke marine engine
Scavenging Process
Computational Fluid Dynamic (CFD) simulation
Reynolds-Averaged Navier-Stokes
Lubrication spray

ABSTRACT

Improving fuel efficiency across all machines is crucial for reducing emissions and lowering energy usage. Automobiles and machinery depend on lubricants to ensure smooth operation and effective energy transfer. In mechanical systems, lubrication is key to minimizing wear between contacting surfaces. While the design of these materials aims for optimal machine performance, wear and tear can decrease efficiency, resulting in higher fuel and energy consumption. This study aims to evaluate how various turbulence methods influence scavenging air dynamics and subsequently affect the interaction between oil spray and scavenging air in a two-stroke engine. In the other words, it is grounded in the essential role of scavenging air in the efficiency and performance of two-stroke engines. This research is significant for its potential to optimize two-stroke engine performance. By better understanding how turbulence influences the interaction between oil spray and scavenging air, it can lead to improved engine designs. Utilizing swirl injection principle (SIP), lubricant injectors spray oil into swirling scavenging air within the cylinder. The study formulates a precise 3D model of uniflow scavenging air, incorporating Reynolds-Averaged Navier-Stokes (RANS) approaches – specifically $k-\varepsilon$ and $k-\omega$ – to simulate turbulence. The research examines flow characteristics during scavenging, comparing predictive performance of $k-\varepsilon$ and $k-\omega$ models in replicating in-cylinder pressure, velocity fields, and spray distribution. Both models reasonably predict in-cylinder pressure and exhibit alignment with experimental data on velocity fields. However, $k-\varepsilon$ excels in tangential velocity prediction. The study analyzes scavenging performance based on operational parameters and examines oil distribution and spreading efficiency using Lagrangian particle distribution. Comparison of contour plots generated by $k-\varepsilon$ and $k-\omega$ simulations with experimental data reveals similarities and differences, particularly in oil mass distribution on the cylinder wall. The $k-\varepsilon$ model demonstrates a broader spray pattern, closer to experimental observations and anticipated behavior, suggesting its superiority in depicting oil spray formation in the two-stroke engine. Therefore, the study recommends the use of the $k-\varepsilon$ turbulence model for more precise simulations.

1. Introduction

Energy conservation and environmental responsibility are gaining importance in various industries. As a major consumer of global fuel, the marine transportation sector is pursuing ways to cut down on fuel consumption and emissions. One strategy involves enhancing engine performance to lower fuel usage and decrease carbon emissions. Research has indicated that friction and wear between engine components are primary causes of energy loss. The relationship between cylinder oil lubrication and fuel in two-stroke marine engines is crucial for maintaining engine efficiency, reducing wear, optimizing fuel economy, and adhering to environmental regulations. Effective management of both fuel and lubrication is key to achieving optimal engine performance and extending the engine's lifespan. Two-stroke diesel engines are pivotal in marine transportation, despite their tendency to emit significant pollutants, notably CO_2 [1,2]. They provide significant benefits, including high efficiency, an excellent power-to-weight ratio, affordability, and dependable performance [3]. In response to stricter regulations set by the International Maritime Organization (IMO) in recent years, significant efforts have been made to develop cleaner and

* Corresponding author.
E-mail address: fra@mp.aau.dk (F. Razavirad).

https://doi.org/10.1016/j.fuel.2024.133042
Received 7 May 2024; Received in revised form 26 August 2024; Accepted 1 September 2024
Available online 6 September 2024

more efficient large two-stroke marine diesel engines [4]. Therefore, the automotive and marine industries have focused on enhancing the understanding of in-cylinder processes to develop engines that are cleaner and more efficient [5]. Other studies have reviewed combustion technologies that have been shown to improve CO2 emissions and the NOx-soot trade-offs, including specific bowl designs, advanced fuel injection systems and clean combustion techniques [6,7]. The scavenging process is essential for the operation of two-stroke engines, significantly influencing overall performance metrics such as power output, fuel consumption, and emissions. Cylinder lubrication oil is critical for engine performance, as it regulates friction and prevents wear. However, it also significantly contributes to the engine ash content. Aabo et al. [8] and Dragsted and Toft [9] emphasizing the need to minimize its consumption for pollution control. Within the cylinder, scavenging flow interacts with oil droplets from the injector and aids in primary spray breakup. Optimizing the scavenging process is crucial for ensuring the efficient evacuation of combustion by-products and the intake of fresh air. This enhancement improves engine efficiency and reduces harmful emissions [10,11]. Various CFD applications are conducted on two-stroke marine diesel engines to gain a deeper understanding of energy distribution and loss [12]. According to the literature, energy analysis of two-stroke marine diesel engines is essential for enhancing the efficiency and performance of these engines [13,14]. In the other words, employing multidimensional numerical simulations, particularly 3D CFD analysis of spray behavior in large two-stroke engines with swirling air, is pivotal for engine research. Such simulations provide valuable insights into fluid dynamics and combustion processes, crucial for optimizing performance, lubrication, fuel efficiency, and emissions. Significant effort has been dedicated to experimental characterization of sprays, particularly those involving liquids such as diesel and gasoline. Insights gained from fuel studies may also have implications for the operation of spray lubrication systems. Initially conducted primarily through experimentation, many researchers have subsequently shifted towards computational modeling [15,16,17,18]. Latest progress have led to a shift towards numerical simulations for studying scavenging in two-stroke marine diesel engines [19,20,21,22,23], marking a departure from experimental investigations on model geometries. Describing spray behavior necessitates addressing intricate multiscale turbulent phenomena that span a broad spectrum of spatial and temporal scales. This complexity stems from the interplay between fluid dynamics, turbulence, droplet formation, breakup, and evaporation. Accurate modeling of these processes demands advanced numerical methods and significant computational resources.

Turbulence modeling encompasses various approaches categorized by flow/grid resolution and computational expense. Direct Numerical Simulation (DNS) resolves all scales, Large Eddy Simulation (LES) captures anisotropic length scales while modeling isotropic/dissipation scales, and Unsteady Reynolds Averaged Navier–Stokes (URANS) relies on ensemble averaging. URANS and LES are commonly used in simulating combustion engines [24]. The comparison between LES and URANS in modeling diesel spray combustion has demonstrated that LES is more effective at capturing certain emission formation phenomena [25] and combustion characteristics [26] than URANS. In URANS, time-averaged Navier–Stokes equations are solved [27], with an isotropic turbulence assumption that might be contentious, especially in swirl and tumble flows [28]. LES applies spatial filtering to the Navier–Stokes equations [27], enabling direct resolution of large vortices crucial for transport. Senecal et al. [29] detailed URANS modeling guidelines for nonevaporating and evaporating scenarios, while subsequent studies examined the impact of high-resolution turbulence methods, particularly LES techniques, on flow field accuracy and cycle-to-cycle variations [30,31]. Habchi and Bruneaux [32] studied LES ensemble averaging effects for single-hole injectors, showing favorable agreements with experimental data. LES is akin to experimental injection requiring ensemble averaging, whereas RANS typically needs a single-shot realization. studies by Lucchini et al. [33] and Yang et al. [34] revealed discrepancies between LES and URANS models in the simulated results of combustion engines and swirling flows. The application of turbulence models in slow-speed marine diesel engines employing uniflow scavenging is crucial for the accurate prediction of in-cylinder flow dynamics. These models enhance the understanding of the complex interactions between air intake, fuel injection, and combustion processes, thereby improving engine efficiency and reducing emissions.

Slow-speed marine diesel engines employ uniflow scavenging, which features inlet scavenging ports and a centrally located exhaust valve at the top of the cylinder. At the bottom of the liner, there are scavenging ports arranged radially. These ports open as the piston reaches the bottom dead center (BDC), thereby exposing them and permitting the flow of scavenging air. The scavenging process is vital for removing combustion by-products and replacing them with fresh air from the scavenging receiver. The scavenging ports are usually angled, often at 20 degrees relative to the radial direction. This angle induces a swirling motion in the incoming fresh air, which improves the scavenging process, aids in cooling the cylinder liner, enhances fuel–air mixing, and assists in lubricating the cylinder liner. Scavenging is influenced by several factors, including engine geometry, the timing of valve and port openings, and the pressure differential between the scavenging receiver and the exhaust duct [35]. Ghazikhani et al. [36] performed an experimental analysis to assess the effects of ethanol additives on the performance of a two-stroke engine, with a particular emphasis on scavenging efficiency. Experimental tests indicate that ethanol blends enhance scavenging efficiency through rapid ethanol evaporation. Additionally, these blends decrease fuel consumption and significantly reduce emissions, particularly carbon monoxide (*CO*) by 35 %. Foteinos et al. [37] created a phenomenological three-zone model for scavenging in two-stroke engines, based on findings from CFD simulations. In a series of studies [38,39,40], Ma et al. [40] investigated different facets of the scavenging process in an opposed-piston diesel engine with a folded cranktrain. The accuracy of the scavenging profile was validated using the tracer gas method. Jia et al. [41] analyzed the effects of valve and scavenging port timing on the performance of a free-piston engine using Ricardo WAVE software. Additionally, several other authors [42,43,44,45] contributed to the enhanced understanding of the two-stroke engine scavenging process. Researchers [19,46,47] performed comprehensive CFD simulations to investigate the scavenging process in a large marine engine. The model was validated by comparing its predictions with in-cylinder velocity measurements obtained using the particle image velocimetry (PIV) technique. Scavenging performance was assessed at various operating points, taking into account different scavenge pressures and scavenging port angles. This study resulted in the creation of a simplified model for predicting the scavenging process in marine two-stroke engines. Efficient operation of internal combustion engines depends on the precise atomization of lubrication injection. This finely atomized lubrication minimizes friction and wear, ensuring smooth engine performance and longevity while reducing the risk of mechanical failure and enhancing overall efficiency.

At high velocities, liquid injection creates a jet that undergoes initial fragmentation, breaking into ligaments and often producing a conical core of liquid close to the nozzle. In other words, the injected liquid at high velocity forms a jet, initiating primary breakup, where the jet splits into ligaments, often forming a conical liquid core near the nozzle. Secondary breakup occurs due to drag forces, breaking the spray into smaller droplets. Atomization, achieved actively or passively, breaks down the jet into a finer spray, crucial in engineering applications such as aerospace propulsion systems and metallurgical processes. Spray breakup, influenced by parameters such as velocity, pressure, nozzle geometry, and fluid properties, is extensively studied using advanced combustion vessels. Multiphase flow analysis employs theoretical, numerical, and experimental methodologies, taking into account turbulent flows and cavitation effects [48,49,50,51,52,53,54,55,56].

To the best of authors knowledge, a comprehensive evaluation of various turbulence models regarding their effectiveness in simulating

scavenging flow and their impact on lubricating oil distribution on cylinder walls within a full-size engine has not been previously explored. This research aims to address this gap by conducting a comprehensive assessment of turbulence models and their implications on the complex dynamics of scavenging flow, specifically focusing on their role in influencing the distribution patterns of lubricating oil on cylinder walls of the engine. Scavenging studies are typically conducted to evaluate scavenging efficiency or optimize port geometry, with the goal of establishing precise initial conditions for subsequent investigations of fuel spray combustion. Given that the geometric investigation of the engine is beyond the scope of this study and the actual geometries of valves, ports, and scavenging receivers are challenging to obtain, a simplified scavenging model has been developed. Therefore, calculating scavenging efficiency without designing the intake port and exhaust duct in a two-stroke marine engine is challenging. In the present study, the scavenging analysis is carried out to obtain more accurate initial conditions for the investigation of lubrication oil spray. Hence, a simplified scavenging model is formulated based on the 4T50ME-X research engine. This study explores scavenging flow in a full-scale, large two-stroke marine engine using URANS turbulence models, specifically $k-\varepsilon$ and $k-\omega$, models. Initial validation of in-cylinder flow is performed against the existing experimental data. The model is then used to examine the distribution and spreading efficiency of the oil within the system. This investigation provides valuable insights into the trajectory of oil droplets within the scavenging flow and identifies the optimal turbulence simulation method to achieve a consistently distributed oil film on the cylinder wall. Furthermore, the present study encompasses the following facets:

- Evaluate the efficacy of various turbulence models in simulating scavenging flow within a full-size two-stroke marine diesel engine.
- Investigate the impact of turbulence models on the distribution patterns of lubricating oil on the cylinder walls during scavenging flow.
- Investigate the dynamics of spray droplets within the scavenging air and their collision with cylinder liner walls and assess the efficacy of the swirl injection principle (SIP) in the context of oil lubrication spray.
- Determine the most suitable turbulence model for achieving a uniformly distributed oil film on the cylinder wall.

The detailed abbreviations and definitions used in this study are listed in Table 1.

2. Methodology

This section provides details regarding the engine specifications, simulation software employed, and the mathematical models utilized to simulate the trajectory of oil droplets during the scavenging process. The comprehensive information presented here serves to establish a foundation for understanding the parameters and methodologies integral to the subsequent analysis of oil droplet dynamics within the studied engine system.

Note that the injection experiments involve the utilization of an HJ E-SIP III injection valve. Fig. 1 presents a schematic illustration of a cylinder featuring six injectors installed on the cylinder liner.

Table 1
List of abbreviation and acronyms used in the study.

Abbreviation	Definition
ATDC	After Top Dead Center
BDC	Bottom Dead Center
CAD	Crank Angle Degree
CFD	Computational Fluid Dynamic
DNS	Direct Numerical Simulation
EVC	Exhaust Valve Close
EVO	Exhaust Valve Open
IPC	Inlet Ports Close
IPO	Inlet Ports Open
LES	Large Eddy Simulation
PIV	Particle Image Velocimetry
RANS	Reynolds-Averaged Navier-Stokes
SIP	Swirl Injection Principle
TDC	Top Dead Center
URANS	Unsteady Reynolds Averaged Navier–Stokes

2.1. Engine specification

The simulations in this study are conducted using the 4T50ME-X research engine. The selection of this particular engine is based on the availability of crucial measurement data, geometric parameters, and relevant operational details accessible to the authors. Table 2 outlines the specifications of the engine. Each cylinder is equipped with a centrally positioned, hydraulically actuated exhaust valve at the top. At the bottom of the liner, 30 scavenging ports are arranged at a 20-degree angle to the radial direction. This deliberate orientation is designed to induce a swirling motion in the incoming fresh air. Noteworthy features of the engine include a turbocharger, and the pressure in the inlet manifold varies based on the engine load. The driving force behind the promotion of scavenging airflow through the cylinder is the pressure differential between the inlet and exhaust manifold.

The engine process begins near the top dead center (TDC) at approximately 0 crank angle degrees (0 CAD). After fuel injection, the fuel mixes with air, starting the complex combustion process. This stage is essential for converting the chemical energy of the fuel into mechanical energy for the crankshaft and is both intricate and critical. Combustion occurs during the expansion phase as the piston moves towards the bottom dead center (BDC). Once combustion is complete, the exhaust valve opens (EVO—exhaust valve open). During the blowdown phase, combustion gases are expelled through the exhaust port due to the pressure difference, as cylinder pressure exceeds that in the exhaust port. As the piston continues to the BDC, pressure decreases. The piston then uncovers the inlet ports (IPO—inlet ports open), allowing fresh air from the scavenging receiver to enter the cylinder through angled ports. This incoming air pushes out the remaining exhaust gases through the exhaust port and aids in cooling the liner. At the end of scavenging, the piston closes the ports (IPC—inlet ports closed), beginning the push-out phase where the air–fuel mixture and residual combustion gases are pushed to the top of the cylinder. Following the closure of the exhaust valve (EVC—exhaust valve closed), a new compression phase begins. The entire process is elucidated in Fig. 2.

2.2. Mathematical models

Turbulence, characterized by recirculation, eddies, and inherent randomness, is scrutinized through CFD approaches. Turbulence models, categorized based on flow resolution, serve as invaluable tools for economically simulating intricate turbulent flows. The foundation of CFD software is rooted in the Navier–Stokes equations. Various models, such as URANS and LES Simulation, collectively form a comprehensive suite, enriching the understanding and application of fluid dynamics. The $k-\varepsilon$ turbulence model, specifically, is one of the most commonly used URANS models, while LES excels in capturing finer details. Direct numerical simulation (DNS), though exhaustive computationally, comprehensively addresses all scales of turbulence. Detached eddy simulation (DES) represents a hybrid approach, combining the merits of URANS and LES methods. The selection of an appropriate turbulence model hinges on the specific application and the desired level of accuracy. Governing equations for simulating scavenging process in two-stroke engines process typically revolve around the conservation principles of mass and momentum. Several factors, including port geometry, piston motion, and gas dynamics, exert considerable influence on the scavenging process. The basic equations employed in simulating the

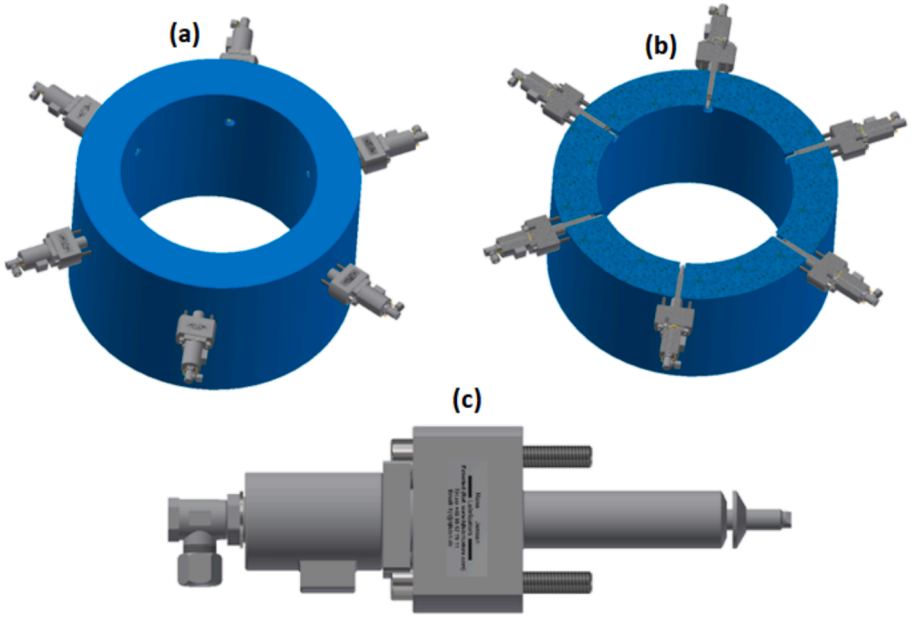

Fig. 1. A) a schematic illustration of a cylinder with six installed injectors on the cylinder liner. b) cross-sectional view of the cylinder featuring six injectors. c) E-SIP valve designed by hans jensen lubricators.

Table 2
Operational conditions and technical specifications for the 4T50ME-X research engine employed in the simulations.

Engine	4T50ME-X
Bore	500 mm
Stroke	2200 mm
Connecting rod	2885 mm
Engine speed	77.5 rpm
Engine load	25 %
Exhaust valve opening	128 CAD ATDC
Exhaust valve closing	257 CAD ATDC
Number of valves	6
Number of Nozzle hole on each injector	1
Number of scavenging ports	30
Scavenging port angle	20 °

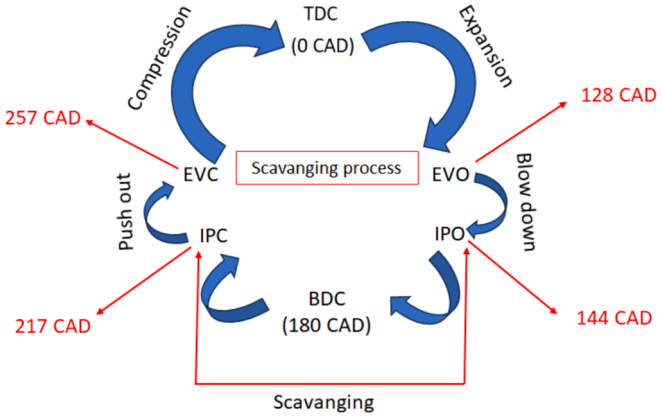

Fig. 2. The process of a uniflow scavenged two-stroke engine.

scavenging process are integral to capturing the dynamic interplay of these factors. These equations serve as the foundation for comprehending and predicting the complex fluid dynamics involved in the movement of gases within the engine cylinder during scavenging.

As mentioned above, turbulence modeling constitutes a critical component in the simulation of fluid flow within internal combustion engines. Among the commonly employed turbulence models, the $k-\varepsilon$ and the $k-\omega$ models stand out for their efficacy. Both models are based on the Reynolds-averaged Navier-Stokes equations and include additional transport equations tailored for turbulence quantities. The governing equations for these commonly used turbulence models are outlined below.

2.2.1. k −ε*Turbulence model*

The turbulence model implemented in this study is the $k-\varepsilon$ model, as proposed by Launder and Spalding [57], which is governed by the following equations:

i) Transport Equation for Turbulent Kinetic Energy.

The transport equation for turbulent kinetic energy (k) defines how turbulent kinetic energy evolves within the flow field and is essential for accurately capturing turbulence effects in CFD simulations. It is typically represented as:

$$\frac{\partial(\rho k)}{\partial t}+\nabla.(\rho k\boldsymbol{u})=\nabla.\left[\left(\mu+\frac{\mu_t}{\sigma_k}\right)\nabla k\right]+P_k-\rho\varepsilon \tag{1}$$

ii) Transport Equation for Specific Dissipation Rate

The transport equation for the specific dissipation rate (ε) is typically expressed as:

$$\frac{\partial(\rho\varepsilon)}{\partial t}+\nabla.(\rho\varepsilon\boldsymbol{u})=\nabla.\left[\left(\mu+\frac{\mu_t}{\sigma_\varepsilon}\right)\nabla\varepsilon\right]+C_{1\varepsilon}\frac{P_k}{\varepsilon}-C_{2\varepsilon}\rho\frac{\varepsilon^2}{k} \tag{2}$$

This equation describes the evolution of the specific dissipation rate, offering insights into the dissipation of turbulent kinetic energy in a CFD simulation using the $k-\varepsilon$ turbulence model.

iii) Turbulent Viscosity.

In the $k-\varepsilon$ turbulence model, the turbulent viscosity (μ_t) is usually calculated using the following relationship:

$$\mu_t=\rho C_\mu\frac{k^2}{\varepsilon} \tag{3}$$

This relation reflects the eddy viscosity concept, where the turbulent viscosity is approximated based on the local turbulence quantities. The constant is typically set to a value around 0.09 in standard imple-

mentations of the $k-\varepsilon$ model. This turbulent viscosity term is crucial for capturing the impacts of turbulence in the fluid flow simulation.

In the equations above, k (in $m^2.s^{-2}$) as the turbulent kinetic energy represents the energy associated with the turbulent fluctuations in velocity. ε (in $m^2.s^{-3}$)) is the specific dissipation rate represents the rate at which turbulent kinetic energy is dissipated per unit volume. μ_t ($kg.m^{-1}.s^{-1}$), the turbulent viscosity, is an artificial viscosity introduced to model the effect of turbulence on the flow. P_k (in $m^2.s^{-3}$) represents the production of turbulent kinetic energy due to mean velocity gradients, $C_{1\varepsilon}$, $C_{2\varepsilon}$, σ_k, σ_ε, C_μ are the turbulence model constant.

2.2.2. k −ω*Turbulence model*

The second turbulence model utilized in this study is the $k-\omega$ models as proposed by Wilcox [58]. The model is governed by the following equations.

i) Transport Equation for Turbulent Kinetic Energy.

The equation below describes the evolution of turbulent kinetic energy within the flow field using the $k-\omega$ turbulence model.

$$\frac{\partial(\rho k)}{\partial t}+\nabla.(\rho k\boldsymbol{u})=\nabla.\left[\left(\mu+\frac{\mu_t}{\sigma_k}\right)\nabla k\right]+2(1-F_1)\rho\omega k+P_k-\beta^*\rho k\omega \quad (4)$$

ii) Transport Equation for Specific Dissipation Rate

The specific dissipation rate (ω) within the flow field using the $k-\omega$ turbulence model is described as follow:

$$\frac{\partial(\rho\omega)}{\partial t}+\nabla.(\rho\omega\boldsymbol{u})=\nabla.[\left(\mu+\frac{\mu_t}{\sigma_\omega})\nabla\omega\right]+2(1-F_2)\frac{\rho\omega^2}{k}-\beta\rho\omega^2 \quad (5)$$

iii) Turbulent Viscosity

In the context of the $k-\omega$ turbulence model, the turbulent viscosity is typically determined using the expression below:

$$\mu_t=\rho\frac{k}{\omega} \quad (6)$$

In the above equations, ω (in s^{-1}), as specific rate of dissipation, represents the rate at which turbulent kinetic energy is dissipated per unit volume. F_1 F_2, β, and β^* are dimensionless model constants. P_k, $\beta^*\rho k\omega$, and $\beta\rho\omega^2$ represent the production of turbulent kinetic energy and its dissipation.

It is imperative to note that the presented equations illuminate the dynamic evolution of turbulent quantities, namely k, ε, and ω, showing their influence on the overall flow field. The solution of these equations, coupled with the standard continuity and momentum equations, affords a comprehensive prediction of turbulent flow characteristics within the engine. It is crucial to emphasize that the choice between employing the $k-\varepsilon$ and $k-\omega$ turbulence models is contingent upon specific flow characteristics and simulation requirements. The selection of an appropriate turbulence model is pivotal in ensuring accurate and meaningful predictions of the turbulent flow dynamics within the engine. Table 3 presents a compilation of the numerical models for scavenging air and spray simulations employed in the current study.

The simulations in this study were conducted using the OpenFOAM software, an open-source finite volume package written in the C++ programming language and designed to tackle the Navier–Stokes equations through the finite volume method [59]. Specifically, the computational fluid dynamics (CFD) numerical framework employed in this investigation is founded on the LibICE code [33], which is built upon the OpenFOAM platform and tailored for internal combustion engines. The simulation dealt with a complex mesh involving a moving piston without the need for intricate mesh manipulation procedures.

Table 3
Investigated numerical models in this study.

Description	Model
Scavenging air modelling	URANS ($k-\varepsilon$) URANS ($k-\omega$)
Initial droplet size distribution	Rosin-Rammler
Secondary liquid breakup	Reitz-Diwakar
Heat transfer for liquid spray	Ranz-Marshall

3. Numerical modelling

3.1. The computational mesh

Dynamic meshing stands as a fundamental technique in CFD and finite element analysis, facilitating the adaptation of the computational grid to changing geometries during simulations. This capability allows for accurate modeling of fluid flow or structural behavior in dynamic scenarios, particularly in fluid–structure interaction situations. In the context of engine simulations, this method involves employing grid deformation techniques such as stretching, smoothing, or morphing to dynamically adjust the mesh as the geometry evolves. For this study, the grid stretching approach is specifically implemented, drawing inspiration from the methodology presented by Launder and Spalding [57]. The dynamic meshing technique for engine simulations requires the mesh to be decomposed as shown in Fig. 3. The cell set layerCells is layered according to the direction of motion, and the algorithm stretches these layers until the thickness tolerance is met. The faces between layerCells and pistonCells are defined as pistonLayerFaces. During expansion, the layerCells stretch depending on the speed of the piston. If the stretching exceeds the thickness tolerance, the layer splits, forming a new layer that continues to stretch. During compression, the layer compresses until it merges with the layer above. This method ensures the mesh maintains quality, as cells above the stretching layer remain unchanged, preserving their stability. When layers split or merge, particle information is smoothly mapped onto the updated mesh, ensuring continuity.

The numerical setup encompasses critical components such as geometry definition, mesh generation, boundary conditions specification, convergence criteria establishment, as well as the selection of solution and discretization schemes. The computational domain takes the form of a 3-dimensional cylindrical space, discretized using the BlockMesh utility.

To verify the accuracy of the results, the simulation undergoes a mesh convergence check. This process involves refining the mesh in three stages, fine mesh, medium mesh and coarse mesh, with each refinement increasing the resolution by approximately the square root of 2 in every direction. Since the focus is on the flow within the cylinder, the averaged angular momentum in the cylinder serves as the convergence parameter. The results of this refinement process are presented in Fig. 4. Based on our preliminary tests and the convergence behavior observed, we believe that the results presented in the study are robust. As illustrated in Fig. 4, the averaged angular momentum demonstrates convergence. The difference between simulations diminishes significantly with successive mesh refinements. Since the medium-sized mesh closely approximates the results of the fine mesh while demanding considerably less computational power, it is selected for further model validation.

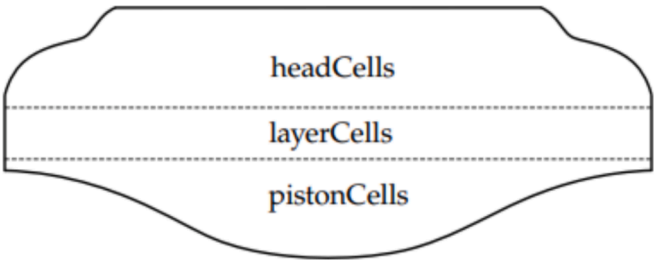

Fig. 3. Illustration of mesh decomposition for the cylinder in the engine simulations at TDC [60].

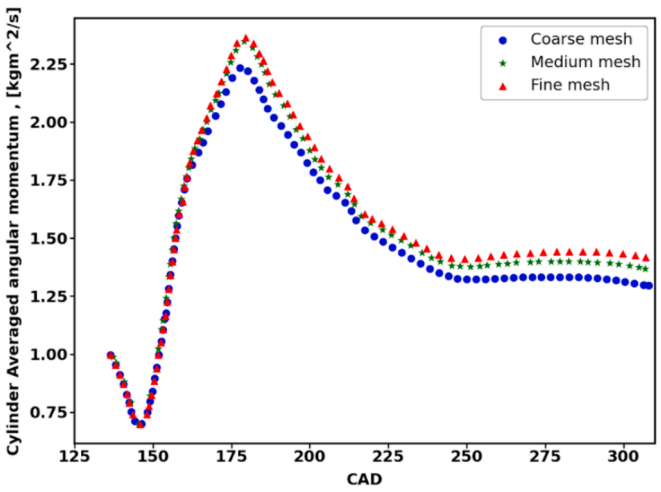

Fig. 4. Cylinder averaged angular momentum for three different refinement levels of the mesh.

The resulting mesh consists of a total of 894,579 elements and 910,872 points, as visually depicted in Fig. 5. OpenFOAM, an open-source finite volume software package, is employed for generating the mesh in this investigation. Despite its lack of a graphical interface, OpenFOAM excels in handling fluid mechanics and diverse physics models, making it a robust choice for simulations requiring dynamic meshing in scenarios such as fluid–structure interaction.

3.2. Scavenging process modelling

The 3D CFD simulation initiates after the exhaust valve opening (EVO) point. The turbulent flow is simulated using URANS approaches, specifically implementing the $k-\varepsilon$ and $k-\omega$ models. Within the scavenging box, the initial species are considered as air, constituting a mixture of nitrogen (N_2) and oxygen (O_2). The initial velocity is defined as a linear distribution commencing from zero in proximity to the walls based on Bessel function. The exhaust exit is modeled with a pressure boundary condition, assigned a time-averaged value of $P_{outlet} = 1.4$ bar. The simulation spans from 138 CAD to 310 CAD to enhance spray

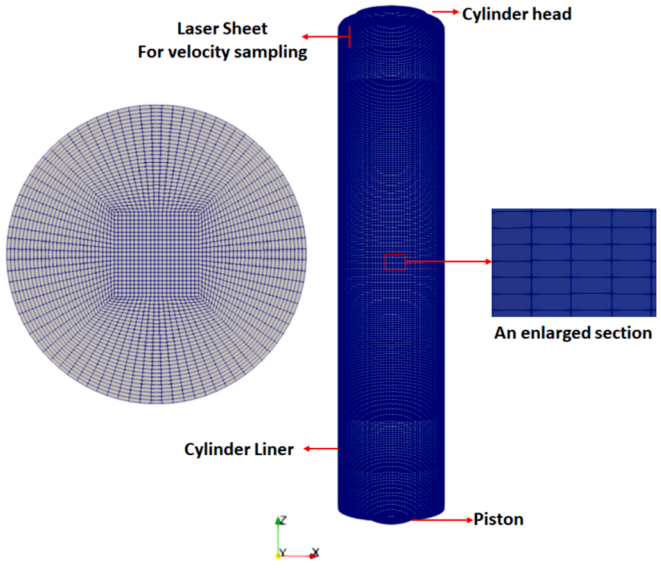

Fig. 5. The computational model includes a detailed view of the mesh. The red vertical line marks the position of the velocity probe, which aligns with the laser sheet and provides optical access for particle image velocimetry (PIV) measurements.

characteristics and achieve a stable flow profile. To ensure stability, the time step size is set to 0.0078125 CAD, keeping the average Courant number for the cylinder below 0.9. Throughout this simulation period, the system attains a steady state and converges. The boundary conditions, internal field settings, and initial conditions employed in the simulation are concisely summarized in Tables 4, 5, and 6, respectively.

Fig. 6 presents a visual representation of the initial and internal fields crucial to the simulation, focusing on key parameters such as velocity and pressure.

3.3. Spray modelling

In spray modeling, two commonly used methodologies are the Eulerian approach, which treats the liquid as a continuous medium or as a secondary phase in multiphase flow, and the Lagrangian approach, which tracks the trajectories of individual droplets [61,62]. Lagrangian models focus on jet and droplet breakup, with primary breakup near the nozzle exit and secondary breakup occurring downstream. These models approximate the jet as a chain of droplets, initially with diameters equal to the nozzle diameter or slightly less, considering cavitation effects if included in the model. In this study, oil spray is directed into the combustion chamber through injectors (Fig. 1), utilizing the Lagrangian parcel distribution. Parcels are injected in a cone shape from the injection point on the liner wall. The applied droplet size distribution model is the Rosin and Rammler model [63], characterized by a doubly-truncated two-parameter Weibull distribution. The injection rate of the oil determined through existing experimental measurements [64]. The injectors are positioned upward to release the oil at a higher elevation, aiming at regions with the greatest wear and lubrication needs. The swirling air motion helps to evenly distribute the lubrication oil over a broader area of the cylinder wall. The interaction with cylinder walls is assumed to result in complete deposition. The mass is recorded on the wall face of the boundary cell where the droplet makes contact, enabling visualization of impact locations [60]. To assess the performance of SIP under low load conditions, the study examines spray motion within the scavenging air, droplet collision with walls, and various turbulence models.

To capture liquid spray and in-cylinder gas interaction, a Lagrangian-parcel Eulerian-fluid method is employed. This signifies that the behavior of individual particles within the liquid spray is tracked using a Lagrangian approach, while simultaneously considering the overall motion of the fluid through an Eulerian approach. Lagrangian particle tracking requires computational resources but provides detailed insights into particle motion. In this study, the droplet size distribution is modeled using a Rosin-Rammler distribution [65], with an injection rate of 20 million parcels per second. Secondary breakup is simulated using the Reitz–Diwakar model [66], and heat transfer is computed using the Ranz–Marshall correlation [67,68]. The working fluid includes fresh air (i.e., O_2 and N_2) and lubricating oil, with their respective properties detailed in Table 7. The model introduces droplets by injecting them in a cone-shaped manner.

4. Results and discussion

4.1. Insights from scavenging process simulation

To validate the simulation, a comparison is performed between the in-cylinder pressure data obtained from the CFD simulation and the experimental measurements taken during the scavenging process. Additionally, the validation process includes the comparison with particle image velocimetry (PIV) results from Hult et al. [70], with a specific focus on axial and tangential velocity components at a location 195 mm from the cylinder axis. Fig. 7 provides a visual representation of the comparison between the anticipated in-cylinder pressure during the scavenging process obtained from the CFD simulation and the corresponding experimental data. The plot in Fig. 7 demonstrates that the

Table 4
Simulation boundary conditions.

	Velocity [ms^{-1}]	Pressure [Pa]	Temperature [K]	$k[m^2s^2]$	$\varepsilon[m^2s^{-3}]$	$\omega[s^{-1}]$
Head	fixedValue	zeroGradient	fixedValue	kqRWallFunction	epsilonWallFunction	omegaWallFunction
Liner	fixedValue	zeroGradient	fixedValue	kqRWallFunction	epsilonWallFunction	omegaWallFunction
Piston	movingWallVelocity	zeroGradient	fixedValue	kqRWallFunction	epsilonWallFunction	omegaWallFunction

Table 5
Initial values of simulation boundary conditions.

	Velocity [ms^{-1}]	Pressure [Pa]	Temperature [K]	$k[m^2s^2]$	$\varepsilon[m^2s^{-3}]$	$\omega[s^{-1}]$
CylinderHead	(0 0 0)	262,600	385	54	28411.2	526.134
Liner	(0 0 0)	262,600	400	54	28411.2	526.134
Piston	(0 0 0)	262,600	510	54	28411.2	526.134

Table 6
Simulation initial conditions.

	Velocity [ms^{-1}]	Pressure [Pa]	Temperature [K]	$k[m^2s^2]$	$\varepsilon[m^2s^{-3}]$	ωs^{-1}
Engine	vector	262,600	628.15	3.02815	24.7389	90.7737

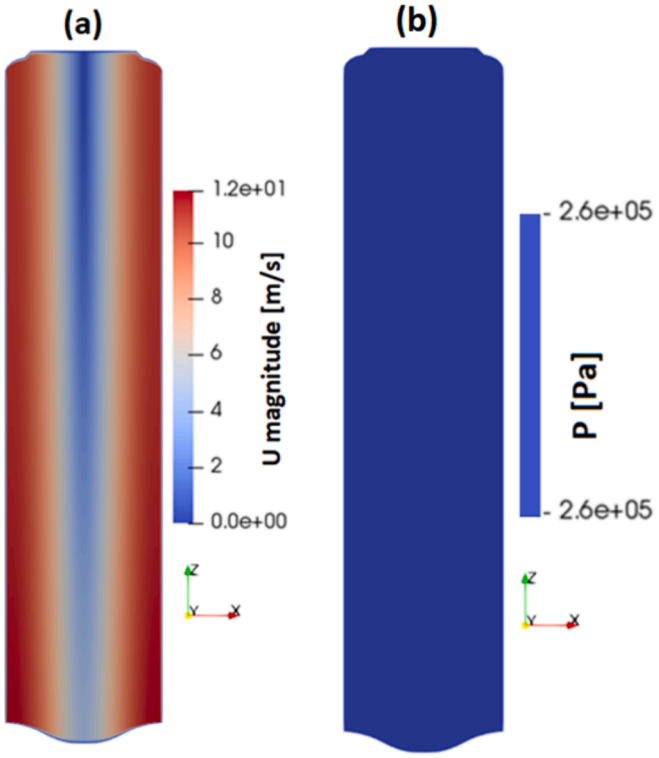

Fig. 6. Simulation initial and internal settings for a) velocity and b) pressure fields.

CFD simulations successfully predict the in-cylinder pressure. However, it is evident that the simulated in-cylinder pressure falls short in capturing the magnitude at 150 CAD and during the period from 220 to 250 CAD. This discrepancy is attributed to the use of a constant outflow boundary condition for pressure, set at 1.4 bar. Consequently, the pressure in the cylinder cannot dip below 1.4 bar, as visibly indicated in the plot. It is important to note that the choice of a constant value of 1.4 bar for the outflow boundary condition for pressure is derived from Nemati et al. [21].

Table 7
Physical properties of the lubrication oil. In the following equations R denotes the ideal gas constant, and T_L represents the temperature of the lubrication oil in degrees Celsius [69].

Property	Value
Density [kgm^{-3}]	$\rho_l(T_L) = (-6.087.10^{-4}.T_L + 0.994)$
Dynamic viscosity [Pa · s]	$\mu_l(T_L) = 0.00610.e^{1246/(R.T_L)}$
Surface tension [N/m]	$\sigma = 0.03$
Vapor pressure [kPa] Derived using the Clausius-Clapeyron equation.	$P_V(T_L) = 10.e^{(A.T_L-B)/((20.T_L+C)).R}$ where A=1094, B=3.458 x10^5, and C=5463.0.
Boiling point [°C]	$T_b = 316$
Base number [mg KOH/g]	BN=70

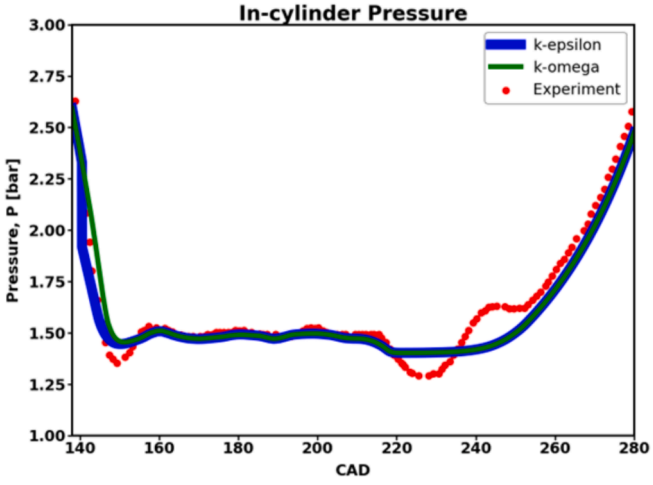

Fig. 7. The in-cylinder pressure during the scavenging process is contrasted with experimental data [70] in the comparison analysis.

It is essential to highlight that the disparity between the $k-\varepsilon$ and $k-\omega$ models in predicting in-cylinder pressure during scavenging is negligible. Consequently, relying solely on pressure validation is insufficient to ensure an accurate representation of the flow inside the cyl-

inder and to compare the performance of the $k-\varepsilon$ and $k-\omega$ modeling approaches. To address this, the velocity flow field forecasted by the present CFD models undergoes validation against experimental data, as depicted in Fig. 8. The axial velocity (velocity along the axis) and tangential velocity (the velocity of rotation around the axis of the cylinder) components are determined by averaging on a surface matching the dimensions of the experimental data and positioned 195 mm away from the axis of the cylinder. Fig. 5 provides a visual representation of the positions for sampling axial and tangential velocities, offering insights into the comprehensive validation process beyond pressure considerations.

As shown in Fig. 8, the CFD simulations accurately predict the evolution of both axial and tangential velocities, demonstrating a reasonable alignment with the experimental data. In other words, the overall shape of the velocity profiles, obtained from both experimental and simulation data ($k-\varepsilon$ and $k-\omega$ models), exhibits remarkable trend similarity. However, Fig. 8 also reveals a discrepancy in the simulated axial velocity, particularly in accurately representing its magnitude at 140 CAD. Additionally, the simulation tends to overestimate the tangential velocity. These turbulence models make certain assumptions and simplifications in predicting fluid flow, and these assumptions may not always capture the complex and detailed characteristics of the flow. Moreover, turbulence models like $k-\varepsilon$ and $k-\omega$ are sensitive to the flow regime, and their performance might vary based on factors such as Reynolds number, flow turbulence intensity, and boundary conditions. The discrepancies between the measured and predicted velocities may be attributed to differences in engine geometries, as the simulation does not account for the exhaust valve. Given that the $k-\varepsilon$ model aligns more closely with the experimental data, it is considered to better predict experimental results. The accuracy of CFD simulations is highly dependent on the quality and resolution of the computational grid. If the grid is not fine enough or if there are issues with grid sensitivity, it can affect the precision of velocity predictions, especially in regions with significant changes or gradients in flow. However, if the experimental data used for validation has uncertainties or variations, it can make it difficult to pinpoint whether discrepancies are due to model limitations or experimental variability.

After the exhaust valve opens, at 128 CAD after top dead center (ATDC), the axial velocity at a point 195 mm from the axial center abruptly increases to around 50 m/s, due to the high flow rate during the blow-down phase (refer to Fig. 2). Once the inlet ports are exposed at the inlet port opening (IPO), the pressure difference across the cylinder decreases, resulting in a significant reduction in axial velocity to approximately 23 m/s. As the scavenging ports gradually open, there is a slight increase in axial velocity, which then stabilizes due to a nearly constant pressure difference between the inlet and exhaust ports. Subsequently, the push-out phase commences after the inlet port closing (IPC), during which the movement of the piston expels gas through the exhaust valve. Around 239 CAD ATDC in the engine cycle, a reduction in flow area occurs, leading to an increase in axial velocity. Following this increase, the exhaust valve closes entirely. Once the valve is fully closed, the axial velocity starts to decrease, causing a slowdown in the airflow along the axis due to the valve closure. It is important to note that the negative axial velocity observed at certain points (CADs) indicates a small backward flow of exhaust gas. This detailed description provides insights into the dynamic changes in axial velocity throughout the engine cycle, capturing the intricacies of the flow phenomena.

Regarding tangential velocity, a distinct peak of approximately 27 m/s occurs around 180 CAD, coinciding with the arrival of the fresh swirling air charge at the measurement position atop the cylinder. Subsequently, the tangential velocity gradually adjusts as the scavenging ports open. This delay is due to the time required for the fresh air from the scavenging ports to reach the measurement area (red vertical line in Fig. 5) near the cylinder head. The simulation is effective in reasonably predicting the time it takes for the tangential velocity to increase. After the sharp increase, the tangential velocity decreases, aligning with the simulation predictions. An intriguing observation is made at around 220 CAD ATDC, where there is a notable increase in tangential velocity. This increase is attributed to the backflow of exhaust gas, immediately enhancing the tangential velocity at the sampling point located below the valve inside the cylinder. This insight provides a comprehensive understanding of the dynamic changes in tangential velocity, considering both the inflow of fresh air and the influence of exhaust gas backflow.

Fig. 9 depicts a significant phenomenon at 158 CAD ATDC, where the incoming air from multiple scavenging ports converges at the center of the cylinder, leading to a noticeable loss of kinetic energy. This occurrence is attributed to heightened radial flow during the scavenging port opening. At 158 and 163 CADs ATDC, three distinct regions within the cylinder exhibit negative axial velocities, identified as recirculation areas: the cylinder bottom near the piston surface, the sidewalls proximate to the cylinder wall, and the central area. In the first region, situated at the bottom near the piston surface, the downward motion of the piston induces a downward pull of exhaust gas, coupled with flow separation and recirculation near the piston surface. The second region, characterized by negative axial velocity, is located in the near-wall zone and is observable across all presented CADs. This phenomenon is likely a result of the separation and recirculation of fresh air above the ports and

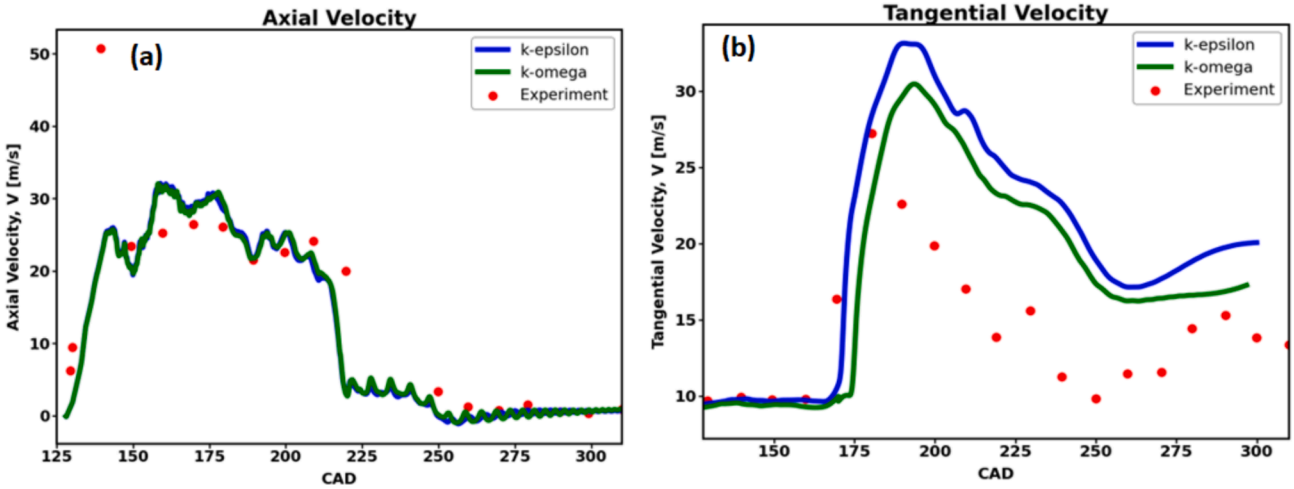

Fig. 8. Illustration of the comparison between (a) axial velocity and (b) tangential velocity from URANS models ($k-\varepsilon$ and $k-\omega$) and the corresponding experimental data derived from [70].

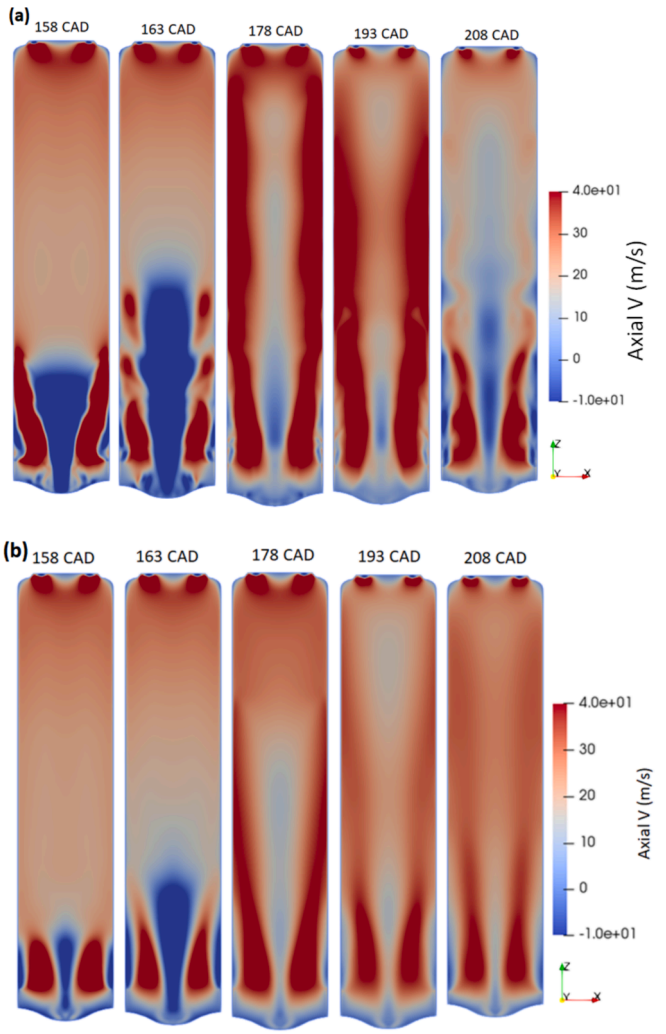

Fig. 9. Axial velocity distribution at various crank angle degrees (CAD) with varied turbulence approaches: (a) URANS ($k-\varepsilon$), (b) URANS ($k-\omega$).

near the cylinder wall. The third region, more pronounced at 163 CAD ATDC, results from an adverse pressure gradient in the center of the cylinder induced by swirl motion, causing a reduction in axial velocity and flow recirculation. This central recirculation region around the cylinder axis leads to vortex breakdown. A comparison of Fig. 9 (a) and 9 (b), obtained using the $k-\varepsilon$ and $k-\omega$ models, respectively, at 163 CAD, reveals differences. The $k-\varepsilon$ model predicts a larger central area with negative axial velocity, while the $k-\omega$ model fails to predict any central recirculation region in the swirl core at 178, 193, and 208 CAD ATDC. This discrepancy is attributed to the incapability of the $k-\omega$ model to simulate highly swirling flows. Although experimental results for this specific engine position in the full-size engine are unavailable, experimental results from a stationary model engine support the existence of central negative axial velocity in this region. Additionally, the velocity field for the $k-\varepsilon$ model exhibits more fluctuations than the $k-\omega$ model, as $k-\omega$ averages all fluctuations, losing the transient large-scale structure of turbulent fluctuation physics.

Fig. 10 depicts the distribution of in-cylinder tangential velocity for both the $k-\varepsilon$ and $k-\omega$ models. At the bottom of the cylinder, the tangential velocity exhibits an increase from the center towards the wall, followed by a decrease near the cylinder wall. This pattern resembles a classic Burgers vortex profile, featuring a central forced vortex surrounded by a peripheral free vortex. Burgers vortex is a mathematical model that describes the flow field of a rotating fluid. It is noteworthy that at 163 CAD ATDC, the high swirl flow does not reach the top of the

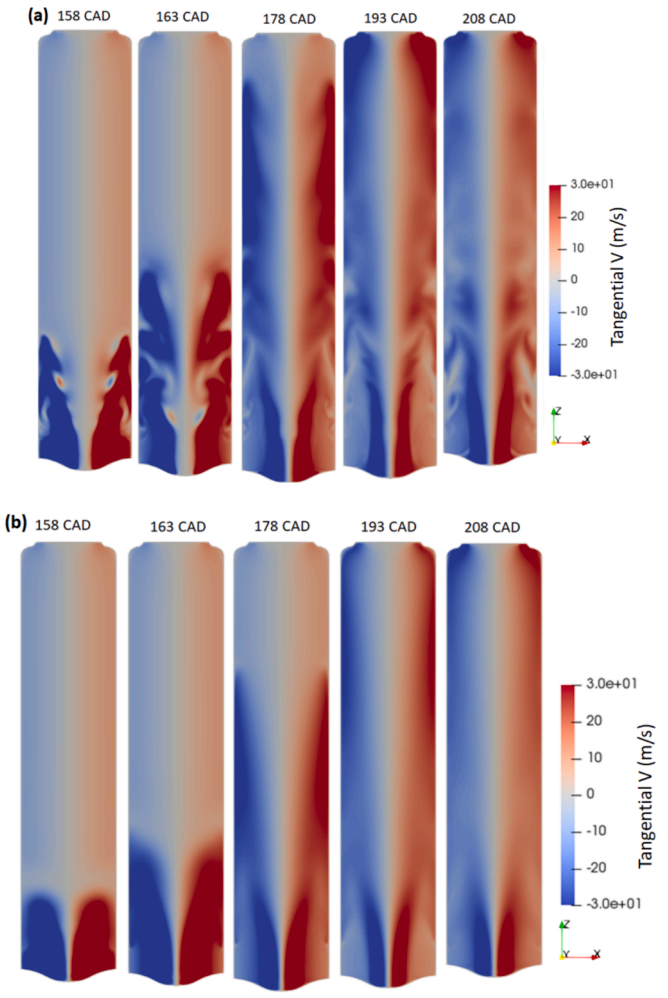

Fig. 10. Tangential velocity distribution at various crank angle degrees (CAD) with varied turbulence approaches: (a) URANS ($k-\varepsilon$), (b) URANS ($k-\omega$).

cylinder, providing an explanation for the consistent tangential velocity observed in Fig. 8b between 138–160 CAD ATDC. A comparative analysis of tangential velocity contours for the $k-\varepsilon$ and $k-\omega$ cases in Fig. 10 reveals that $k-\varepsilon$ predicts a more extended region of Burgers vortex upstream of the cylinder compared to $k-\omega$, particularly at 193 and 208 CAD ATDC.

4.2. Assessing the impact of turbulence models on oil distribution across the liner

To assess the effectiveness of the SIP process under low load conditions, an analysis is conducted to examine the influence of different turbulence models on spray formation and mass storage on the wall. In order to evaluate the precision of the spray model, the spray simulation is compared with experimental work conducted by Lauritsen et al. [71]. The experiments were conducted in a wind tunnel designed to replicate in-cylinder flow during the injection period. As depicted in Fig. 1, six valves are strategically arranged around the cylinder liner, with a presumed nozzle tip angle of 60 degrees, and the valves oriented outward at an angle of 45 degrees. In the context of spray-wall interaction, the assumption is made that every droplet hitting a wall completely deposits on it. A contour plot, obtained from the simulation, indicating the mass distribution on the cell faces, is generated, as illustrated in Fig. 11. The Figure is presented from an external perspective, treating the cylinder liner as transparent.

This analysis aims to provide insights into the agreement between

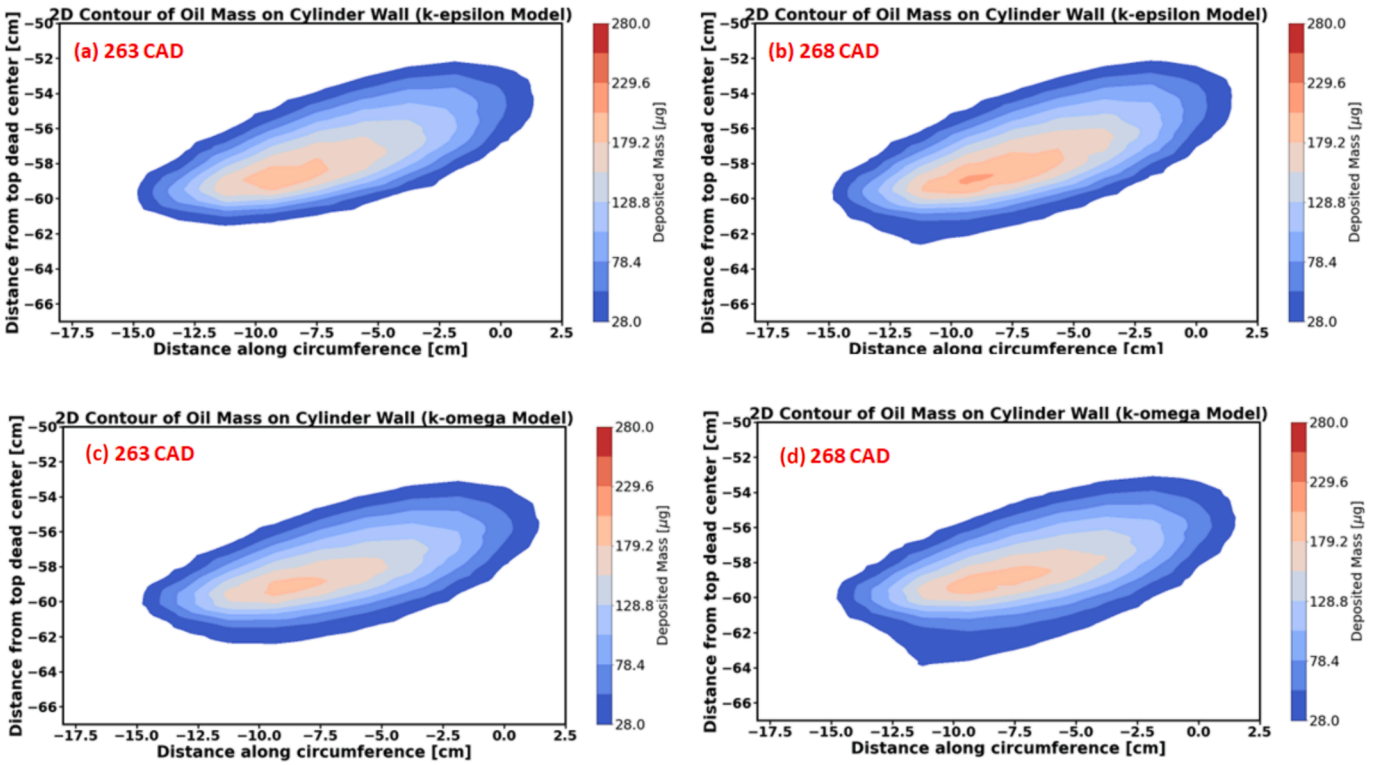

Fig. 11. Contour representation depicting the distribution of oil mass on the cylinder wall as simulated with $k-\varepsilon$ and $k-\omega$ methods. (a) and (b) $k-\varepsilon$ models for 263 and 268 CADs, respectively. (c) and (d) $k-\omega$ models for 263 and 268 CADs, respectively. The warmer color corresponds to varying thickness levels, with warmer sahde indicating a thicker oil layer.

simulation results and experimental data, specifically focusing on the distribution of mass on the cylinder walls under the influence of different turbulence models. As illustrated in Fig. 11, the mass distribution is concentrated towards the left side of the contour. The originally curved contour is flattened for a 2D presentation. The contour aligns with the spray direction and appears circular when viewed from the injection point on the curved surface.

The elongation observed in the contour is attributed to the extended travel of smaller droplets, while larger droplets, traveling shorter distances, are less influenced by this effect. The leftward concentration of mass is attributed to the upward-angled left-to-right injection direction. This visualization provides a clear representation of the spatial distribution of mass on the cylinder walls, offering valuable insights into the spray dynamics under the influence of the SIP process. The comparison between the modeled contour in Fig. 11 and the experimental one in Fig. 12 reveals both similarities and differences. Both contours depict mass concentration on the left, corresponding to the impact zone of larger droplets. The contours exhibit alignment in a consistent direction, aligning seamlessly with both the injection direction and the flow orientation at the moment of injection. Despite having a similar width, the experimental contour is more elongated due to factors not considered by the model. Firstly, droplets colliding with a high Weber number surface result in some mass being re-injected as secondary droplets, contributing to elongation. This effect may explain a larger light blue section on the right in Fig. 12. Secondly, differences in cylinder bore size between the simulation (500 mm) and experiment (900 mm) introduce disparities in the data. These observations highlight the importance of considering additional factors in the simulation, such as secondary droplet formation upon collision with surfaces of high Weber number, and the impact of variations in cylinder bore size. Despite these differences, the overall alignment between the modeled and experimental contours indicates a reasonable representation of the spray-wall interaction under the selected simulation conditions.

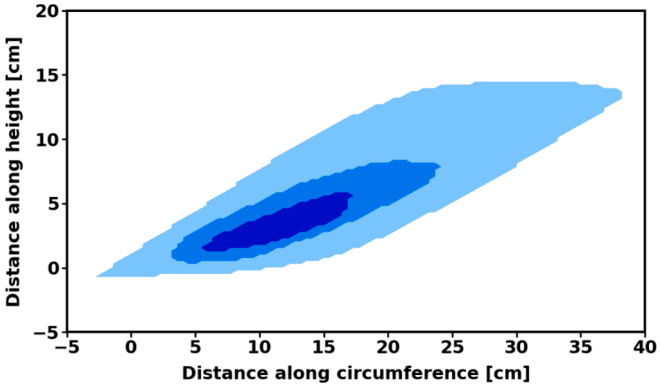

Fig. 12. Contour depicting the oil mass distribution on the wind tunnel wall, simulating realistic in-cylinder flow. Darker shade corresponds to increased oil layer thickness.

4.2.1. *Comparison of $k-\varepsilon$ and $k-\omega$ turbulence models*

The study undertakes a comparative analysis of the performance of URANS models, specifically $k-\varepsilon$ and $k-\omega$, in simulating scavenging flow. This examination extends to evaluating their impact on spray formation and mass storage on the cylinder wall within a full-size engine context. Given the crucial role of the scavenging process in affecting air–fuel mixing and combustion, ensuring the precision of flow simulations in these engines is essential. Fig. 11 illustrates the representation of the $k-\varepsilon$ and $k-\omega$ models at two distinct injection times, specifically during lubrication injection at 263 CAD and the subsequent injection at 268 CAD. Evidently, the contour plots for both models exhibit a consistent shape at two distinct injection times. Nevertheless, a noticeable disparity emerges in the height of the spray spread. Utilizing the $k-\varepsilon$ model, as depicted in Fig. 11 (a) and (b), the spray disperses at a greater height where the wear is most pronounced. Contour plots of oil

distribution on the cylinder wall resulting from simulations using the $k-\varepsilon$ and $k-\omega$ turbulence models were compared with experimental data obtained from experimental work conducted by Lauritsen et al. [71]. The focus is on assessing the shape of the oil mass storage on the cylinder wall. Upon visual inspection, notable differences in the shape of the oil mass storage were observed between the two turbulence models. The $k-\varepsilon$ model exhibited a spray spread with higher elevation, particularly in areas corresponding to elevated wear regions on the cylinder liner. This observation suggests that the $k-\varepsilon$ model predicts a broader and potentially more realistic oil distribution pattern in regions prone to increased wear.

Quantitative measures were obtained to further assess the differences. Maximum oil thickness, spread area, and other relevant metrics were considered. Statistical analysis revealed significant variations in the predicted oil mass storage between the $k-\varepsilon$ and $k-\omega$ models. The $k-\varepsilon$ model consistently showed higher values for these metrics, indicating a more extensive spray pattern. The observed differences in the shape of the oil mass storage are crucial for understanding the potential wear patterns on the cylinder liner. The ability of the $k-\varepsilon$ model to predict a spray spread at higher elevations aligns with physical expectations in areas prone to heightened wear. This suggests that the $k-\varepsilon$ turbulence model may provide a more accurate representation of oil spray formation in the studied context. The configuration of the most substantial oil layer (depicted in dark orange) at 268 CAD in the $k-\varepsilon$ model exhibits a notable resemblance to the thickest of the oil layer observed in the experimental study (illustrated in dark blue in Fig. 12). The results from both turbulence models were assessed for physical plausibility. The spray patterns were compared to established fluid dynamics principles, and discrepancies were scrutinized. The capability of the $k-\varepsilon$ model to capture a broader spray aligns with the expected physics of oil dispersion, further supporting its potential superiority in this application. In conclusion, the comparison between the $k-\varepsilon$ and $k-\omega$ turbulence models highlight distinct differences in the shape of oil mass storage on the cylinder wall. The $k-\varepsilon$ model, with its broader spray pattern, appears to better align with experimental data and physical expectations. Therefore, based on this analysis, it is suggested that the $k-\varepsilon$ turbulence model may offer a more accurate representation of oil spray formation in the studied cylinder liner-piston interaction. Acknowledging the limitations of this study, such as potential simplifications in the models and uncertainties in experimental data, prompts consideration for future research. Subsequent studies could explore refinements in turbulence models or incorporate additional factors to further enhance the accuracy of oil spray simulations in similar contexts.

5. Conclusion

Optimizing cylinder lubrication oil distribution offers potential benefits including reduced oil consumption, decreased wear, and enhanced cylinder condition. This optimization contributes to lower particle emissions, aiding vessels in meeting regulatory standards. Multidimensional numerical simulations, particularly 3D CFD analysis, offer valuable insights for improving efficiency and minimizing wear in large two-stroke engines. This study has scrutinized the predictive capabilities of $k-\varepsilon$ and $k-\omega$ models in simulating in-cylinder pressure during scavenging, highlighting the negligible disparity between their realizable outcomes. However, it highlighted the limitations of relying solely on pressure validation for understanding flow dynamics. To address this, the velocity flow field, validated against experimental data, emerged as a crucial metric. The comparison of axial and tangential velocities revealed a substantial alignment between simulation and experiment, emphasizing the reliability of both $k-\varepsilon$ and $k-\omega$ models. Noteworthy discrepancies, such as an overestimation of tangential velocity, were detailed throughout the engine cycle, providing insights into the complex interplay of forces governing flow phenomena. Visualizations of axial and tangential velocity fields at various crank angles offered a deeper understanding of spatial flow patterns and recirculation zones. These findings contribute to advancing the comprehension of in-cylinder fluid dynamics, thereby informing and refining computational models for enhanced predictive accuracy in internal combustion engine simulations. The comparison between $k-\varepsilon$ and $k-\omega$ turbulence models has illuminated notable disparities in the distribution of oil mass on the cylinder wall. The $k-\varepsilon$ model, characterized by a broader spray pattern, exhibits a closer alignment with both experimental observations and anticipated physical behavior. Consequently, from the findings of this analysis, it is recommended that the $k-\varepsilon$ turbulence model provides a more precise depiction of oil spray formation in the examined two-stroke engine. While recognizing the inherent limitations of this study, including potential simplifications in the models and uncertainties in experimental data, it underscores the need for future investigations. In the quest for advancing the understanding of oil spray simulations within analogous contexts, future research endeavors could explore avenues beyond the confines of current turbulence models. Refining existing turbulence models, introducing additional parameters, and considering alternative models such as LES turbulence models present promising directions to enhance the precision of these simulations. The exploration of LES, with its ability to capture finer turbulent scales, could provide valuable insights into the intricacies of oil spray dynamics in cylinder liner-piston interactions.

CRediT authorship contribution statement

Flora Razavirad: Writing – original draft, Validation, Software, Methodology, Investigation, Formal analysis. **Bjørn Christian Dueholm:** Software, Methodology, Conceptualization. **Nikolaj Kristensen:** Supervision, Funding acquisition. **Jesper de Claville Christiansen:** Supervision, Funding acquisition.

Declaration of competing interest

The authors declare that they have no known competing financial interests or personal relationships that could have appeared to influence the work reported in this paper.

Data availability

Data will be made available on request.

Acknowledgements

The investigation, which produced these findings, was financially supported by Hans Jensen Lubricators A/S and the Innovation Fund Denmark under grant no. 3197-00002A. The authors would like to express their sincere gratitude to Dr. Martin M.B Bak for his invaluable contributions to this study. His expertise, insightful feedback, and support were instrumental in enhancing the quality and depth of our research.

References

[1] Becagli S, et al. Evidence for heavy fuel oil combustion aerosols from chemical analyses at the island of Lampedusa: a possible large role of ships emissions in the Mediterranean. Atmos Chem Phys 2012;12(7):3479–92. https://doi.org/10.5194/acp-12-3479-2012.

[2] Petzold A, Weingartner E, Hasselbach J, Lauer P, Kurok C, Fleischer F. Physical Properties, Chemical Composition, and Cloud Forming Potential of Particulate Emissions from a Marine Diesel Engine at Various Load Conditions. Environ Sci Technol May 2010;44(10):3800–5. https://doi.org/10.1021/es903681z.

[3] Cong Y, Gan H, Wang H. Parameter investigation of the pilot fuel post-injection strategy on performance and emissions characteristics of a large marine two-stroke natural gas-diesel dual-fuel engine. Fuel 2022;323:124404. https://doi.org/10.1016/j.fuel.2022.124404.

[4] Nemati A, Ong JC, Pang KM, Mayer S, Walther JH. A numerical study of the influence of pilot fuel injection timing on combustion and emission formation under two-stroke dual-fuel marine engine-like conditions. Fuel 2022;312:122651. https://doi.org/10.1016/j.fuel.2021.122651.

[5] Ong JC, Walther JH, Xu S, Zhong S, Bai X-S, Pang KM. Effects of ambient pressure and nozzle diameter on ignition characteristics in diesel spray combustion. Fuel 2021;290:119887. https://doi.org/10.1016/j.fuel.2020.119887.

[6] Liu J, Dumitrescu CE. Numerical Investigation of Methane Number and Wobbe Index Effects in Lean-Burn Natural Gas Spark-Ignition Combustion. Energy Fuel May 2019;33(5):4564–74. https://doi.org/10.1021/acs.energyfuels.8b04463.

[7] Liu J, Dumitrescu CE. 3D CFD simulation of a CI engine converted to SI natural gas operation using the G-equation. Fuel 2018;232:833–44. https://doi.org/10.1016/j.fuel.2018.05.159.

[8] K. Aabo, J. P. Liddy, K. C. Lim, and S. L. Moore, "2-Stroke Crosshead Engine Cylinder Lubrication — the Future Here Today," in *23rd CIMAC World Congress*, 2001.

[9] Dragsted J, Toft O. "Influence of low cylinder consumption on operating cost for 2-stroke engine", in *CIMAC Congress*. Kyoto 2004.

[10] W. H. Percival, "Method of Scavenging Analysis for 2-Stroke-Cycle Diesel Cylinders," *SAE Transactions*, vol. 63, pp. 737–751, 1955, [Online]. Available: http://www.jstor.org/stable/44468606.

[11] Sher E, Hossain I, Zhang Q, Winterbone DE. Calculations and measurements in the cylinder of a two-stroke uniflow-scavenged engine under steady flow conditions. Exp Therm Fluid Sci 1991;4(4):418–31. https://doi.org/10.1016/0894-1777(91)90005-C.

[12] Lu Z, et al. Numerical research of the in-cylinder natural gas stratification in a natural gas-diesel dual-fuel marine engine. Fuel 2023;337:126861. https://doi.org/10.1016/j.fuel.2022.126861.

[13] Wang D, Zhang H, Qian Y, Deng K. Experimental energy and exergy analysis of turbocharged marine low-speed engine with high pressure exhaust gas recirculation. Fuel 2022;323:124360. https://doi.org/10.1016/j.fuel.2022.124360.

[14] H. Zhang *et al.*, "Experimental Study of the Influences of Operating Parameters on the Performance, Energy and Exergy Characteristics of a Turbocharged Marine Low-Speed Engine," *Processes*, vol. 11, no. 10, 2023, doi: 10.3390/pr11102924.

[15] Ling Y, Zaleski S, Scardovelli R. Multiscale simulation of atomization with small droplets represented by a Lagrangian point-particle model. Int J Multiph Flow 2015;76:122–43. https://doi.org/10.1016/j.ijmultiphaseflow.2015.07.002.

[16] Edelbauer W, Birkhold F, Rankel T, Pavlovic Z, Kolar P. Simulation of the Liquid Break-up at an AdBlue Injector with the Volume-of-Fluid method followed by Off-Line Coupled Lagrangian Particle Tracking. Comput Fluids Sep. 2017;157. https://doi.org/10.1016/j.compfluid.2017.09.003.

[17] Heinrich M, Schwarze R. 3D-coupling of Volume-of-Fluid and Lagrangian particle tracking for spray atomization simulation in OpenFOAM. SoftwareX Jan. 2020;11:100483. https://doi.org/10.1016/j.softx.2020.100483.

[18] Zhou H, Xiang M, Zhao S, Weihua Z. Development of a multiphase cavitation solver and its application for ventilated cavitating flows with natural cavitation. Int J Multiph Flow May 2019;115:62–74. https://doi.org/10.1016/j.ijmultiphaseflow.2019.03.020.

[19] Andersen F, Hult J, Nogenmyr K-J, Mayer S. Numerical Investigation of the Scavenging Process in Marine Two-Stroke Diesel Engines. SAE Technical Papers Nov. 2013;11. https://doi.org/10.4271/2013-01-2647.

[20] Lamas MI, Vidal C. Computational Fluid Dynamics Analysis of the Scavenging Process in the MAN B&W 7S50MC Two-Stroke Marine Diesel Engine. J Ship Res Sep. 2012;56:154–61. https://doi.org/10.5957/JOSR.56.3.120001.

[21] Nemati A, Ong JC, Jensen MV, Walther JH, Pang KM, Mayer S. "Numerical Study of the Scavenging Process in a Large Two-Stroke Marine Engine Using URANS and LES Turbulence Models", in *SAE Powertrains, Fuels & Lubricants Meeting*. SAE International Sep. 2020. https://doi.org/10.4271/2020-01-2012.

[22] T. Senčić, V. Mrzljak, V. Medica-Viola, and I. Wolf, "CFD Analysis of a Large Marine Engine Scavenging Process," *Processes*, vol. 10, no. 1, 2022, doi: 10.3390/pr10010141.

[23] Sigurdsson E, Ingvorsen KM, Jensen MV, Mayer S, Matlok S, Walther JH. Numerical analysis of the scavenge flow and convective heat transfer in large two-stroke marine diesel engines. Appl Energy 2014;123:37–46. https://doi.org/10.1016/j.apenergy.2014.02.036.

[24] Fink G, Jud M, Sattelmayer T. Influence of the spatial and temporal interaction between diesel pilot and directly injected natural gas jet on ignition and combustion characteristics. J Engng Gas Turbines Power 2018.

[25] Zhang M, Ong JC, Pang KM, Bai X-S, Walther JH. An investigation on early evolution of soot in n-dodecane spray combustion using large eddy simulation. Fuel 2021;293:120072. https://doi.org/10.1016/j.fuel.2020.120072.

[26] Lu Z, Zhou L, Ren Z, Lu T, Law CK. Effects of Spray and Turbulence Modelling on the Mixing and Combustion Characteristics of an n-heptane Spray Flame Simulated with Dynamic Adaptive Chemistry. Flow Turbul Combust 2016;97(2):609–29. https://doi.org/10.1007/s10494-015-9702-5.

[27] Belgiorno G, Di Blasio G, Beatrice C, Fraioli V, Migliaccio M. Experimental Evaluation of Compression Ratio Influence on the Performance of a Dual-Fuel Methane-Diesel Light-Duty Engine. SAE Int J Engines Sep. 2015;8(5):2253–67. https://doi.org/10.4271/2015-24-2460.

[28] Mavrelos C, Theotokatos G. Numerical investigation of a premixed combustion large marine two-stroke dual fuel engine for optimising engine settings via parametric runs. Energy Convers Manag Jan. 2018;160. https://doi.org/10.1016/j.enconman.2017.12.097.

[29] P. Senecal, E. Pomraning, K. Richards, and S. Som, "Grid-Convergent Spray Models for Internal Combustion Engine CFD Simulations," in *Proceedings of the ASME 2012 Internal Combustion Engine Division Fall Technical Conference (ICEF2012-92043)*, 2012.

[30] P. K. Senecal *et al.*, "Large Eddy Simulation of Vaporizing Sprays Considering Multi-Injection Averaging and Grid-Convergent Mesh Resolution," *J Eng Gas Turbine Power*, vol. 136, no. 11, May 2014, doi: 10.1115/1.4027449.

[31] Q. Xue, S. Som, P. K. Senecal, and E. Pomraning, "A Study of Grid Resolution and SGS Models for LES under Non-reacting Spray Conditions," 2013. [Online]. Available: https://api.semanticscholar.org/CorpusID:131771243.

[32] C. Habchi and G. Bruneaux, "LES and Experimental investigation of Diesel sprays," 2012. [Online]. Available: https://api.semanticscholar.org/CorpusID:54751671.

[33] Lucchini T, D'Errico G, Jasak H, Tukovic Z. "Automatic Mesh Motion with Topological Changes for Engine Simulation", in *SAE World Congress & Exhibition*. SAE International Apr. 2007. https://doi.org/10.4271/2007-01-0170.

[34] R. Yang, G. Theotokatos, and D. Vassalos, "Parametric investigation of a large two-stroke marine high-pressure direct injection engine by using computational fluid dynamics method," *Proceedings of the Institution of Mechanical Engineers, Part M: Journal of Engineering for the Maritime Environment*, vol. 234, p. 147509021989563, Jan. 2020, doi: 10.1177/1475090219895639.

[35] J. B. Heywood, *Internal Combustion Engine Fundamentals*, 2nd Edition. New York: McGraw-Hill Education, 2018. [Online]. Available: https://www.accessengineeringlibrary.com/content/book/9781260116106.

[36] Ghazikhani M, Hatami M, Safari B, Ganji DD. Experimental investigation of performance improving and emissions reducing in a two stroke SI engine by using ethanol additives [Online]. Available: Propul Power Res 2013;2:276–83. https://api.semanticscholar.org/CorpusID:67754664.

[37] M. I. Foteinos, A. Papazoglou, N. Kyrtatos, A. Stamatelos, O. Zogou, and A.-M. Stamatellou, "A Three-Zone Scavenging Model for Large Two-Stroke Uniflow Marine Engines Using Results from CFD Scavenging Simulations," *Energies (Basel)*, 2019, [Online]. Available: https://api.semanticscholar.org/CorpusID:164991660.

[38] Ma F, Zhao C, Zhang F, Zhao Z, Zhang S. Effects of Scavenging System Configuration on In-Cylinder Air Flow Organization of an Opposed-Piston Two-Stroke Engine. Energies (Basel) 2015;8(6):5866–84. https://doi.org/10.3390/en8065866.

[39] Ma F, et al. Simulation Modeling Method and Experimental Investigation on the Uniflow Scavenging System of an Opposed-Piston Folded-Cranktrain Diesel Engine. Energies (Basel) 2017;10(5). https://doi.org/10.3390/en10050727.

[40] Ma F, Zhang L, Su T. Simulation Modeling and Optimization of Uniflow Scavenging System Parameters on Opposed-Piston Two-Stroke Engines. Energies (Basel) 2018;11(4). https://doi.org/10.3390/en11040940.

[41] Jia B, Wang Y, Smallbone A, Roskilly AP. Analysis of the Scavenging Process of a Two-Stroke Free-Piston Engine Based on the Selection of Scavenging Ports or Valves. Energies (Basel) 2018;11(2). https://doi.org/10.3390/en11020324.

[42] Rueter D. 2-Stroke Scavenging in Conventional and Minimally-Modified 4-Stroke Engines for Heavy Duty Applications at Low to Medium Speeds. Inventions 2019;4(3). https://doi.org/10.3390/inventions4030044.

[43] Ciampolini M, Bigalli S, Balduzzi F, Bianchini A, Romani L, Ferrara G. CFD Analysis of the Fuel-Air Mixture Formation Process in Passive Prechambers for Use in a High-Pressure Direct Injection (HPDI) Two-Stroke Engine. Energies (Basel) 2020;13(11). https://doi.org/10.3390/en13112846.

[44] Qiao Y, Duan X, Huang K, Song Y, Qian J. Scavenging Ports' Optimal Design of a Two-Stroke Small Aeroengine Based on the Benson/Bradham Model. Energies (Basel) 2018;11(10). https://doi.org/10.3390/en11102739.

[45] Grljušić M, Tolj I, Radica G. An Investigation of the Composition of the Flow in and out of a Two-Stroke Diesel Engine and Air Consumption Ratio. Energies (Basel) 2017;10(6). https://doi.org/10.3390/en10060805.

[46] F. Andersen, J. Hult, K.-J. Nogenmyr, and S. Mayer, "CFD Analysis of the Scavenging Process in Marine Two-Stroke Diesel Engines," *ASME 2014 Internal Combustion Engine Division Fall Technical Conference, ICEF 2014*, vol. 1, Oct. 2014, doi: 10.1115/ICEF2014-5438.

[47] Andersen F, Mayer S. Parametric Study of the Scavenging Process in Marine Two-Stroke Diesel Engines 2015. https://doi.org/10.1115/ICEF2015-1075.

[48] V. Champagne Jr, S. Dinavahi, and P. Leyman, "Prediction of Particle Velocity for the Cold Spray Process," Jan. 2011.

[49] B. M. Hanrahan and C. M. Waits, "Fabrication and Testing of Tapered Electro-spray Nozzles," 2012. [Online]. Available: https://api.semanticscholar.org/CorpusID:55622159.

[50] C.-B. M. Kweon, "A Review of Heavy-Fueled Rotary Engine Combustion Technologies," 2011. [Online]. Available: https://api.semanticscholar.org/CorpusID:110643792.

[51] Bardi M, et al. Engine combustion network: Comparison of spray development, vaporization, and combustion in different combustion vessels. Atomization Sprays Jan. 2012;22:807–42. https://doi.org/10.1615/AtomizSpr.2013005837.

[52] T. Bazyn and G. C. Martin, "Spray Combustion Measurements in a Flow-Through High Temperature, High Pressure Chamber," in *23rd Annual Conference on Liquid Atomization and Spray Systems*, Ventura, May 2011.

[53] Bruneaux G, et al. Comparison of Diesel Spray Combustion in Different High-Temperature, High-Pressure Facilities. SAE Int J Engines Oct. 2010;3(2):156–81. https://doi.org/10.4271/2010-01-2106.

[54] Faeth GM, Hsiang L-P, Wu P-K. Structure and breakup properties of sprays. Int J Multiph Flow 1995;21:99–127. https://doi.org/10.1016/0301-9322(95)00059-7.

[55] L. Pickett, "Introducing the Engine Combustion Network," in *International Multidimensional Engine Modeling User's Group Meeting at the SAE Congress*, Detroit, Apr. 2008.

[56] Lin S, Reitz R. Drop and spray formation from a liquid jet. Annu Rev Fluid Mech Nov. 2003;30:85–105. https://doi.org/10.1146/annurev.fluid.30.1.85.

[57] Launder BE, Spalding DB. The numerical computation of turbulent flows. Comput Methods Appl Mech Eng 1974;3(2):269–89. https://doi.org/10.1016/0045-7825(74)90029-2.

[58] Wilcox DC. Reassessment of the scale-determining equation for advanced turbulence models [Online]. Available: AIAA J 1988;26:1299–310. https://api.semanticscholar.org/CorpusID:119826448.
[59] H. K. Versteeg and W. Malalasekera, "An_Introduction_to_Computational_Fluid_D".
[60] Dueholm BC. Cylinder Spray Lubrication of Two-Stroke Diesel Engines: Investigation of Scavenging Air, Droplet Movement and Nozzle Flow. Aalborg University; 2024.
[61] M. Archambault, "Stochastic Spray Flow Models: A Review," in *ILASS-Americas 22nd Annual Conference on Liquid Atomization and Spray Systems,* Cincinnati, May 2010.
[62] Pai M, Subramaniam S. Accurate numerical solution of the spray equation using particle methods. Atomization and Sprays - ATOMIZATION SPRAYS Jan. 2006;16:159–94. https://doi.org/10.1615/AtomizSpr.v16.i2.30.
[63] Crenin F. Truncated Weibull Distribution Functions and Moments. SSRN Electron J 2015.
[64] B. Dueholm, J. deClaville Christiansen, B. Endelt, and N. Kristensen, "Injection rate of cylinder lubrication oil in large two-stroke marine diesel engines using a common rail lubrication system," 2023. [Online]. Available: https://api.semanticscholar.org/CorpusID:259375590.
[65] Ranz WE. Evaporation from drops [Online]. Available: Chem Eng Prog 1952;48:142–80. https://api.semanticscholar.org/CorpusID:112688807.
[66] Reitz RD, Diwakar R. "Effect of Drop Breakup on Fuel Sprays", in *SAE International Congress and Exposition*. SAE International Feb. 1986. https://doi.org/10.4271/860469.
[67] Pang KM, Karvounis N, Walther JH, Schramm J. Numerical investigation of soot formation and oxidation processes under large two-stroke marine diesel engine-like conditions using integrated CFD-chemical kinetics. Appl Energy 2016;169:874–87. https://doi.org/10.1016/j.apenergy.2016.02.081.
[68] Chishty MA, Bolla M, Hawkes ER, Pei Y, Kook S. Soot formation modelling for n-dodecane sprays using the transported PDF model. Combust Flame 2018;192:101–19. https://doi.org/10.1016/j.combustflame.2018.01.028.
[69] Ravendran R, Endelt B, Christiansen J, Jensen P, Theile M, Najjar I. Coupling method for internal nozzle flow and the spray formation for viscous liquids. International Journal of Computational Methods and Experimental Measurements Mar. 2019;7:130–41. https://doi.org/10.2495/CMEM-V7-N2-130-141.
[70] J. Hult, S. Matlok, and S. Mayer, "Particle Image Velocimetry Measurements of Swirl and Scavenging in a Large Marine Two-Stroke Diesel Engine," in *SAE 2014 World Congress & Exhibition*, SAE International, Apr. 2014. doi: 10.4271/2014-01-1173.
[71] S. Lauritsen, J. Dragsted, and B. Buchholz, "Swirl Injection Lubrication - a New Technology To Obtain Low Cylinder Oil Consumption Without Sacrificing Wear Rates," in *CIMAC Congress*, 2001, pp. 921–932.